Supporting Information

Enhancing ionic conductivity and suppressing Li dendrite formation in lithium batteries using a vinylene-linked covalent organic framework solid polymer electrolyte

Jin Yang[a,#], Chenxiao Lin[b,e,#], Yonglei Wang[b], Yaolin Xu[b], Duong Tung Pham[a], Xiangqi Meng[b], Khanh Van Tran[b], Sijia Cao[b,d], Nikolay Kardjilov[b], André Hilger[b], Jan Dirk Epping[a], Ingo Manke[b], Arne Thomas[a,*], Yan Lu[b,c,d,*]

[a]Department of Chemistry/Functional Materials Technische Universität Berlin, Hardenbergstraße40, 10623 Berlin (Germany)

[b]Department of Electrochemical Energy Storage Helmholtz-Zentrum Berlin für Materialien und Energie, Hahn-Meitner-Platz1, 14109 Berlin (Germany)

[c]Institute for Technical and Environmental Chemistry,Friedrich-Schiller-Universität Jena, Philosophenweg 7b, 07743 Jena

[d]Helmholtz Institute for Polymers in Energy Applications (HIPOLE), Philosophenweg 7b, 07743 Jena

[e]College of New Energy, Ningbo University of Technology, Ningbo University of Technology, 315336 Ningbo (China)

[#]Jin Yang and Chenxiao Lin contributed equally to this work.

Corresponding author:

Prof. Dr. Yan Lu: yan.lu@helmholtz-berlin.de

Prof. Dr. Arne Thomas: arne.thomas@tu-berlin.de

1 Material and characterization methods

1.1 Materials

All the reagents and solvents used for the synthesis were commercially available and used without further purification. The mesitylene (1,3,5-trimethylbenzene, >98%), MeOH (methanol, 99%) were purchased from Sigma Aldrich Chemicals. LiTFSI (Lithium Bis(TrifluoromethanesulfonyI)imide, Sigma Aldrich) and PEO (polyethylene oxide, $M_W = 1\times10^6$ or 10^5 Da, Sigma Aldrich), PVDF (poly (vinylidene fluoride), Sigma Aldrich), and the precursors such as ethyl acitimidate hydrochloride (ABCR, 99%) and terepthalaldehyde (Sigma Aldrich, 99%) were purchased and used as received. All aqueous solutions were prepared with DI water produced from the Millipore purification system.

1.2 Characterization methods

1.2.1 Powder X-ray diffraction (PXRD) analysis

Powder X-ray diffraction data were collected on a Bruker D8 Advance diffractometer in reflection geometry operating with a Cu Kα anode (λ = 1.54178 Å) operating at 40 kV and 40 mA. Samples were ground and mounted as loose powders onto a Si sample holder. PXRD patterns were collected from 2 to 60 2θ degrees with a step size of 0.02 degrees and an exposure time of 2 seconds per step. For air-sensitive samples, the samples were loaded on an air-tight holder in the glovebox and measured immediately after being transferred out of the glovebox.

1.2.2 Scanning electron microscope (SEM)

The SEM analyses of COF samples were performed on an S-2700 scanning electron microscope (Hitachi, Tokyo, Japan).

1.2.3 Transmission electron microscopy (TEM)

COF samples for TEM were sonicated in ethanol for 10 min and a 4 μL of sample dispersion was applied to Lacey carbon-coated copper TEM grids (200 mesh, Science Services) and subsequently dried under a fume hood. Imaging was performed on JEM-2100 (JEOL GmbH, Eching, Germany) operated at 200 kV and equipped with a 4 k × 4 k CMOS digital camera (TVIPS TemCam-F416).

1.2.4 Fourier transform infrared spectroscopy (FTIR) analyses

The Fourier transform infrared spectroscopy (FTIR) analyses of the samples were carried on a Varian 640IR spectrometer equipped with an ATR cell.

1.2.5 X-ray photoelectron spectroscopy (XPS)

XPS was measured on K-Alpha™ + X-ray Photoelectron Spectrometer System (Thermo Scientific) with Hemispheric 180° dual-focus analyzer with 128-channel detector. X-ray monochromator is Micro focused Al-K_α radiation. For the measurement, the prepared powder samples were pressed and loaded on carbon taps, then pasted onto the sample holder for measurement. The data was collected with an X-ray spot size of 400 μm, 20 scans for the survey, 50 scans for the specific regions, and 100 scans for the valance band (VB) regions.

1.2.6 Solid-state NMR (ss-NMR) measurements

^{7}Li solid-state NMR magic-angle spinning (MAS) and ^{13}C cross-polarization magic angle spinning (CPMAS) spectra were carried out on a Bruker Avance 400 MHz spectrometer operating at 100.6 MHz and 155,4 MHz for ^{13}C and ^{7}Li, respectively. The experiments were carried out at a MAS rate of 10 kHz using a 4 mm MAS HX double-

resonance probe with two pulse phase modulation (TPPM) proton decoupling was used during acquisition. The T_1 value of ^{7}Li was measured using a saturation recovery pulse sequence with 100-500 saturation pulses in the saturation pulse train and recovery times varying from 0.05 s to 5000 s. The T_1 was obtained according to the formula:

$$I = I_0(1 - \exp(-t / T_1))$$

where I is the peak intensity at time t, I_0 is the saturation intensity and T_1 is the longitudinal relaxation constant.

1.2.7 Physisorption measurements

Nitrogen (N_2) sorption analyses were conducted at 77 K using an Autosorb-iQ-MP from Quantachrome. The pore size distributions were calculated from the adsorption isotherms by quenched solid density functional theory (QSDFT) using the slit pore model for carbon adsorbents. Before analysis, samples were degassed at 120 °C for 12 h. BET surface areas were determined over a 0.05-0.1 p/p_0 range.

1.2.8 Thermogravimetric analysis (TGA)

TGA measurements were carried out under Nitrogen enviroment on a Mettler Toledo TGA 1 Stare thermal instrument with a heating rate of 5 K min^{-1}.

1.2.9 Dynamic differential calorimetry (DSC) measurement

The phase transition behaviors of the VCOF-SPE and Ref-SPE were determined by a differential scanning calorimeter (Netzsch 200 F3). The samples are cooled from room temperature to -60 °C and equilibrated at -60 °C for 30 min before collecting data. The heating scan was started from -60 °C to 200 °C with a heating rate of 10 K min^{-1}.

1.2.10 Tensile tests

All the samples for tensile tests were cut into rectangular strips with a width of 3 mm and lengths of 30 mm by a razor blade. Mechanical tensile tests were conducted on an Instron 5960 universal testing machine (Instron, USA) at room temperature. Tensile strength and failure strain were recorded when the fracture occurred. Young's modulus was calculated from the slope of the linear region of the stress-strain curves.

2. Materials preparation

2.1 Synthesis of VCOF-1

Vinylene-Linked Covalent Organic Frameworks[1]: 2,4,6 trimethyl s-triazine was synthesized by following the reported procedures[1]. A Teflon-lined steel autoclave (23 mL, Parr instrument) was charged with 2,4,6 trimethyl s-triazine (TMT) (73.8 mg, 0.6 mmol), terepthalaldehyde (TA) (120.69 mg, 0.9 mmol), NaOH (105 mg), methanol (14mL) and mesitylene (2mL). The autoclave was sealed and placed in a preheated oven at 180 °C for 3 days. After three days, the autoclave was cooled down and the formed precipitate was collected by filtration and thoroughly washed with water, methanol, and acetone. VCOF-1 was obtained as a fluffy yellow powder after a further drying step under vacuum at 100 °C. It is noted that the samples should avoid prolonged exposure to light to prevent cycloaddition reactions[1]. Isolated yield: 83% (135 mg).

2.2 Preparation of VCOF-SPE and Ref-SPE

VCOF solid polymer electrolyte (VCOF-SPE): Appropriate quantities of LiTFSI (Lithium Bis(Trifluoromethanesulfonyl)imide) and polyethylene oxide (PEO, M_W = $1*10^6$) for EO to Li^+ ratio 8:1 were dissolved in 5 mL acetonitrile. Then 3.85 wt% of VCOF-1 and 9.6 wt% of poly (vinylidene fluoride) (PVDF) were added and homogeneously stirred for 24 hours at room temperature. Afterward, the obtained slurry was cast on a Teflon plate and dried inside the Argon glove box for 7 days. The

thickness of the free-standing polymer electrolyte film was tuned at approximately 200 μm, denoted as VCOF-SPE. PVDF was introduced as an enhancement to the mechanical properties of the SPEs. The incorporation of PVDF aimed to address the issue of stickiness and difficulty in peeling off SPEs prepared solely from PEO and LiTFSI, particularly when adhered to the PTFE plate. In addition, PVDF also reduces the crystallinity of PEO and thereby enhances the mobility of Li ions[2].

3. Electrochemical Measurements

3.1 Coin-cell assembly and test parameters

Cells were facially assembled by 2032 coin-cell types with layers of the active-material electrode (f16 mm), VCOF-SPE (f18.0 mm), and lithium foil (f16 mm). The working electrodes were prepared by mixing the active material $LiFePO_4$ (LFP) (70%), Super P (10%), and 5wt% solution of PEO (20%, M_w=10^5 Da). The mixture was placed in a Fritsch planetary ball mill and mixed for 30 min (600 rpm) to obtain a homogeneous slurry, which was then uniformly coated onto a carbon-coated Aluminum foil (battery grade) current collector. The electrode mass loading was tuned at 1.5 mg/cm^2. The LFP/VCOF-SPE/Li half-cell measurements were performed within the potential range of 2.5 to 4.0 V (vs. Li/Li^+) at different current densities. Galvanostatic studies were performed on the coin cell type assembled in an argon-filled glove box using a programmable battery tester (Interface 1010E, Gamry).

3.2 *In-situ* X-ray computed tomography (MicroCT) and galvanostatic measurements

The ionic conductivities of the prepared VCOF-SPE membrane were characterized by in-situ MicroCT in combination with electrochemical impedance spectroscopy (EIS).

X-ray Tomography measurements were conducted on the Li/VCOF-SEP/Li Tomo-cell in the original state (25ºC) and after several heating steps to 30, 40, 50, 60, and 70 °C[3]. The detailed design and configuration of the cell are thoroughly sketched in the figure shown below. The temperature was controlled and stabilized several hours before measurements by a thermal amplifier. Full frequency range impedance spectra from 1 MHz to 0.01 Hz were measured during CT scanning as the cell was stabilized at preset temperature conditions. A reference solid electrolyte was also prepared without VCOF-1 for comparison, denoted as Ref-SPE.

The X-ray imaging facility built at Helmholtz-Zentrum Berlin (HZB) consisted of an X-ray tube (Hamamatsu, L8121-03) and a flat panel detector (Hamamatsu, C7942SK-05). This device produces a cone beam from the microfocus X-ray source which allows adjusting the field of view and the spatial resolution when the source-detector-distance (SDD) and source-object-distance (SOD) were changed. These laboratory X-ray tomographic measurements were performed using the X-ray tube voltage of 80 kV and current of 125 µA and the source-to-sample and source-to-detector distances are 70 and 600 mm, respectively. 1000 projections were recorded during the rotation of 360º with the exposure time of 2.1 s and 3 frames. For this setup, the obtained resolution is 5.83 µm/voxel in the samples.

The lithium stripping/platting process in combination with MicroCT measurements was further conducted on both VCOF-SPE and Ref-SPE samples after 0, 150, 200, and 300 hours cycling. The applied current and working temperature were set at 0.1 mA/cm^2 and 60 °C throughout the measurements, respectively.

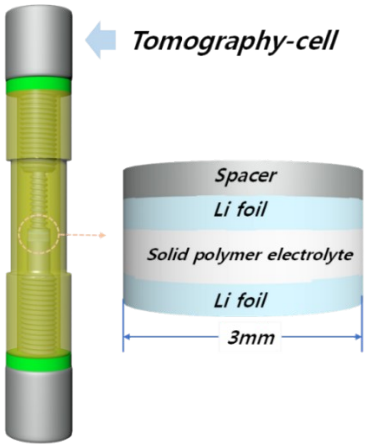

Figure S1. Configuration of the tomography-cell

The calculation of the thickness of the SPE layers is based on different X-ray attenuation coefficients of different materials. For this purpose, samples will be located in front of the detector system to record transmission images. The obtained raw datasets were normalized using Darkfield and Flatfield images by the ImageJ software.[4] To ensure the accuracy of the calculation, the thickness was calculated at five different rotation angles, and on each angle, five different positions were chosen for computing. It should be noted that the operating temperature was slightly changed due to long-time measurement in the ambient environment. Therefore, the sample temperature was carefully controlled and monitored by a thermal infrared camera to minimize the influence of working condition variation.

3.3 Li^+ transference number

The Li^+ transference number (t^+_{Li}) of the SPE at 60 °C was determined by the alternating current AC/ direct current DC technique using the symmetrical cell of Li|VCOF-SPE|Li, which had been invented by Bruce and Vincent[5,6]. The DC polarization voltage of 10 mV was applied to the prepared cell. Before and after the DC polarization, the cell's impedance spectra were performed in the frequency range from 1 MHz to 0.01 Hz. Both electrochemical measurements and DC polarization were

performed using the Gamry instrument. The operating temperature was maintained at 60 °C by using an Arbin's Cell-Isolating Thermal Safety Chamber. The Li^+ transference number (t_{Li}^{+}) of the DTP-SPE was calculated by the equation:

$$t_{Li}^{+} = \frac{I_s(\Delta V - I_0 R_0)}{I_0(\Delta V - I_S R_S)} \quad (1)$$

Where I_0 and I_s are initial current and steady current values, ΔV is the applied potential in the DC method, R_0 and R_s are the interfacial resistance of the electrolyte film before and after DC polarization obtained from the EIS analysis, respectively.

3.5 Pouch cell assembly and abuse test

Large format lithium-ion polymer solid electrolyte was carried out using pouch-cell consisting of LFP as the positive electrode (active mass: 29.2 mg), a VCOF-SPE film as the electrolyte, and lithium metal laminated on an aluminum current collector as the negative electrode. The electrode size was optimized as 57 x 44 mm, while the solid electrolyte film is larger ~ 2 mm in each dimension. The cell was then facially constructed by the stacking method between layers. All components were vacuumed and hot sealed inside an aluminum laminated film cover. Finally, the pouch-cell pressure was retained by a homemade clamping tool to ensure the optimum contact of electrolyte/electrode interfaces.

LFP/VCOF-SPE/Li pouch cells were connected to a red light-emitting diode (LED). The abuse tests were performed at room temperature in the air. A stainless-steel needle was used to penetrate the pouch cell in the nail penetration test, and stainless-steel scissors were applied to cut more than half of the pouch cell during the cutting test. Optical photographs were recorded to show the results of abuse tests.

4. Density Functional Theory (DFT) Calculations

DFT calculations were performed using GAUSSIAN 16 package to obtain optimized molecular structures of single absorbents and their specific coordinations with representative fragments of VCOF-1 structures. Molecular geometry optimizations were carried out at the B3LYP/6-311+G(d,p) level of theory with explicit Grimme's-D3 dispersion correction, which is appropriate over medium (≈2−5 Å) and long ranges (>5 Å), and is an effective method to obtain binding structures of complexes with reduced computational cost. Multiple starting configurations of the nicotine molecule were optimized. Each of these was validated with no negative vibrational eigenvalues in harmonic frequency analysis. The binding energy E_{bind} was calculated via $E_{bind} = E_{Ion\text{-}VCOF\ complexes} - E_{Ion} - E_{VCOF}$, in which E_{Ion}, $E_{VCOF,}$ and $E_{Ion\text{-}VCOF\ complexes}$ are the total energies of absorbed ion molecules (Li-ions, TFSI anions, PEO fragments, *etc.*), representative VCOF-1 fragments, and Ion-VCOF-1 complexes, respectively. A more negative value of E_{bind} indicates a much stronger interaction of ion molecules with VCOF-1 fragments.

5. Atomistic simulations

Atomistic simulations of systems with and without VCOF-1 materials were performed using the GROMACS package. The modeling system consisting of 200 LiTFSI ion pairs, 400 PEO (n=4) chains, 30 PVDF (n=10) chains, and 15 COF fragments (the same structure as we used in DFT calculations) was constructed, and a reference simulation system without VCOF-1 fragments was also constructed for a comparative purpose. The equations for the motion of all atoms were integrated using a classic Verlet leapfrog integration algorithm with a time step of 1.0 fs. A cutoff radius of 1.6 nm was set for short-range van der Waals interactions and real-space electrostatic interactions. The

particle-mesh Ewald (PME) summation method with an interpolation order of 5 and a Fourier grid spacing of 0.15 nm was employed to handle long-range electrostatic interactions in reciprocal space. All simulation systems were first energetically minimized using a steepest descent algorithm and thereafter annealed gradually from 600 K to room temperature (300 K) within 15 ns. All annealed simulation systems were equilibrated in an isothermal-isobaric (NPT) ensemble for 25 ns of physical time maintained using a Nosé-Hoover thermostat and a Parrinello-Rahman barostat with time coupling constants of 0.4 and 0.2 ps, respectively, to control the temperature at 300 K and the pressure at 1 atm. Atomistic simulations were further performed in a canonical ensemble (NVT) for 50 ns, and simulation trajectories were recorded at an interval of 100 fs for further structural and dynamical analysis.

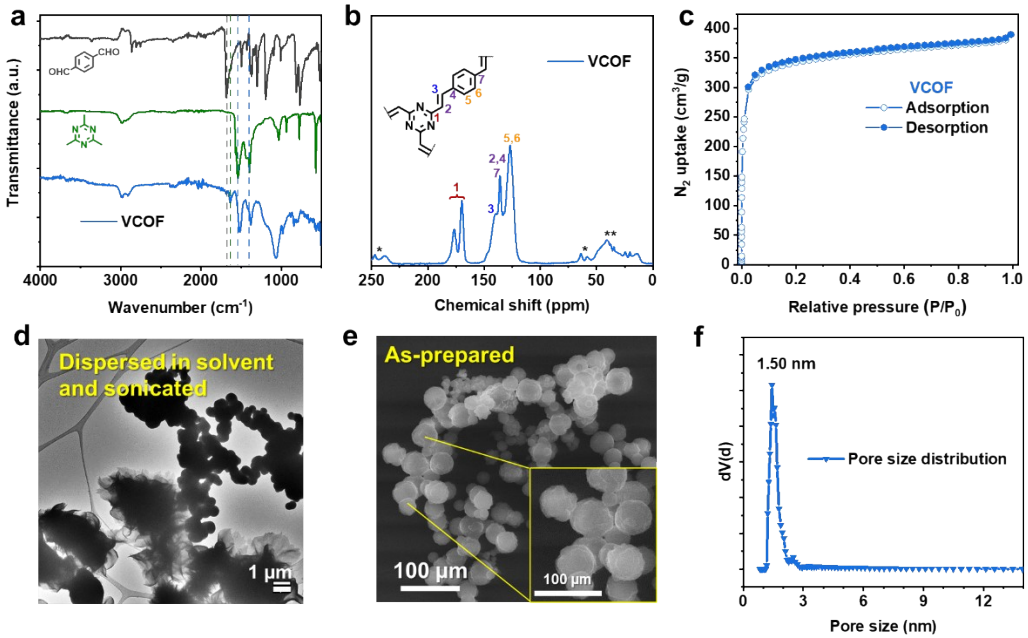

Figure S2. (a) FTIR of the monomers and the VCOF-1. (b) ^{13}C ss-NMR spectra, (c) N_2 sorption data, (d) TEM image, (e) SEM image of VCOF-1. (f) Fitted pore size distribution of VCOF-1 is based on the N_2 sorption data.

In Figure S2, the FTIR peaks at ~ 3000 cm^{-1} are assigned to the C-H Alkyl stretching.

The different morphologies from the TEM and SEM images originated from the different sample preparation methods. For TEM measurement, VCOF-1 was dispersed in ethanol and thoroughly sonicated before drop-casting onto the TEM grid. The sonication exfoliated the 2D VCOF-1 layers which made the layered substructure to be visualized. For SEM measurement, the VCOF-1 was directly pasted on the SEM sample holder which made the VCOF-1 preserve its pristine macro morphology.

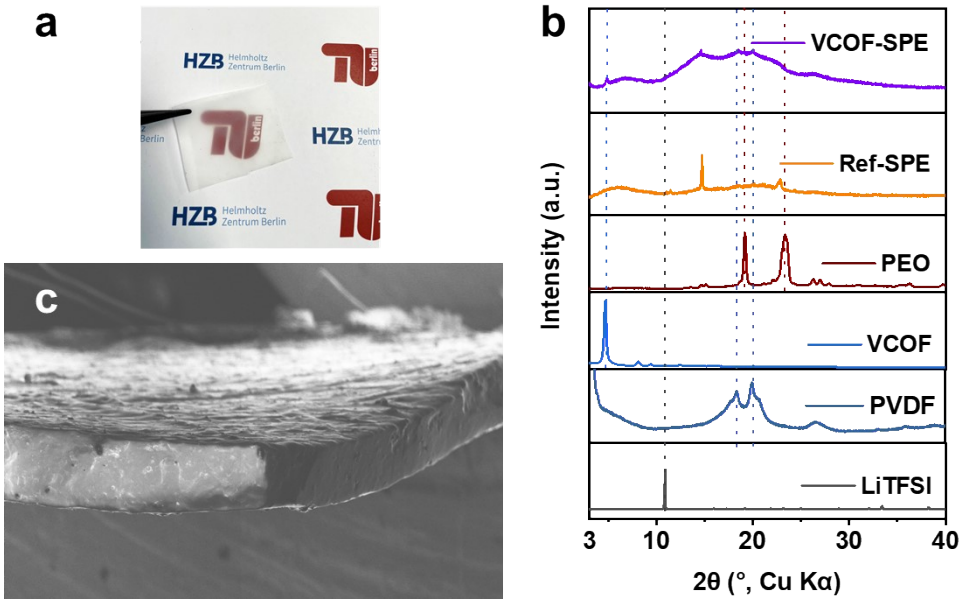

Figure S3. (a) Photograph of the prepared Ref-SPE. (b) Comparison of the PXRD patterns of LiTFSI, PVDF, VCOF-1, PEO, and VCOF-SPE. (An air-tight holder was applied for the XRD measurements.) (c) Full SEM image of the prepared VCOF-SPE.

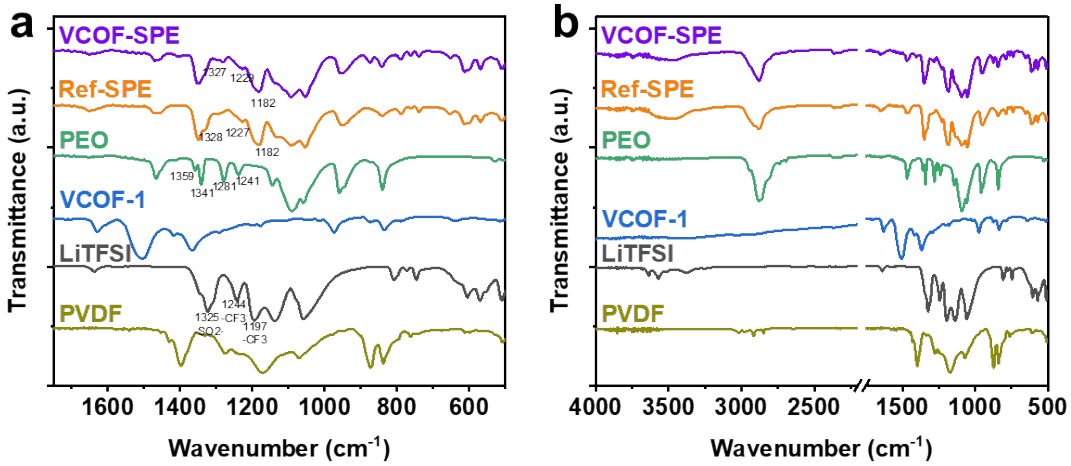

Figure S4. FTIR spectra of PVDF, LiTFSI, VCOF-1, PEO, Ref-SPE, and VCOF-SPE at (a) 1700 - 500 cm^{-1} and (b) the full spectra.

The $-CH_2-$ peaks in PEO at 1359, 1341, 1281, and 1241 cm^{-1} can be easily detected in Ref-SPE and VCOF-SPE. But the peaks at 1359 and 1341 cm^{-1} merge to one peak with the $-SO_2-$ the peak of LiTFSI[7].

Table S1. FTIR peaks and assignments for VCOF-SPE, Ref-SPE, PEO, LiTFSI.

	Wavenumber (cm^{-1})			
	PEO	LiTFSI	Ref-SPE	VCOF-SPE
-CH_2- wagging absorptions in the helical structure	1359	-	1359	1359
-CH_2- wagging absorptions in trans planar structure	1341	-	1341	1341
-CH_2- twist in the helical structure	1281	-	1281	1281
-CH_2- twist in trans planar structure	1241	-	1241	1241
Asymmetric -SO_2- stretching	-	1325	1328	1327
Symmetric stretching of -CF_3	-	1244	1227	1229
Asymmetric stretching of -CF_3	-	1197	1182	1182

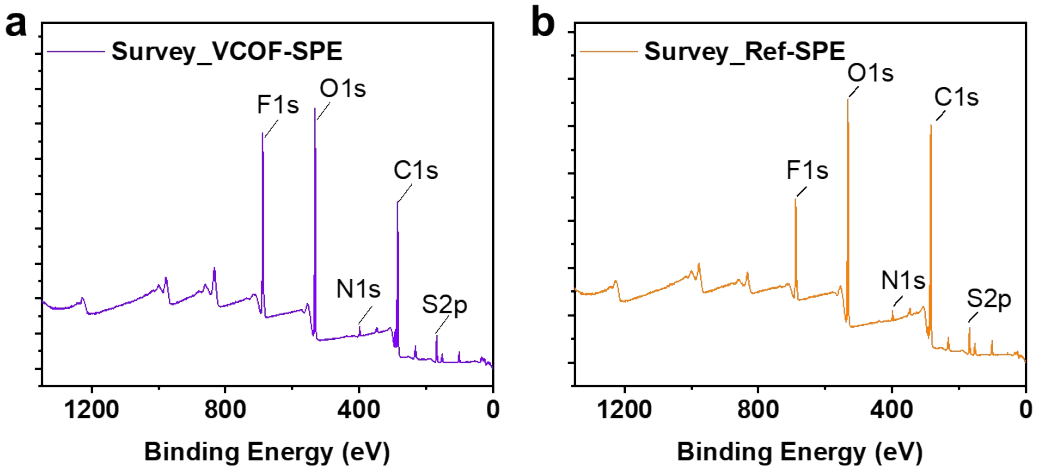

Figure S5. XPS survey spectra of VCOF-SPE and Ref-SPE.

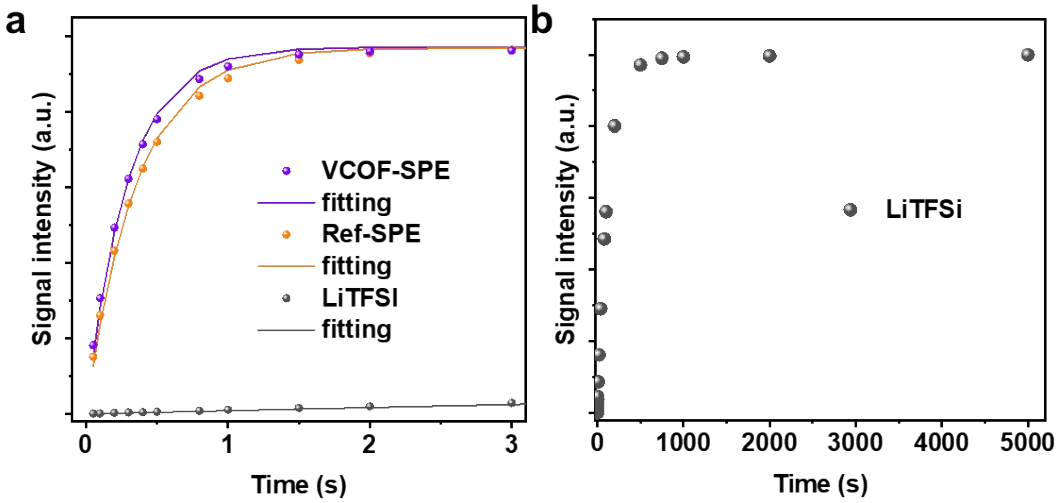

Figure S6. (a) Comparison of the saturation recovery plot from ^{7}Li ss-NMR MAS spectra of VCOF-SPE, Ref-SPE, and LiTFSI. (b) The full range of the spectra of LiTFSI.

The T_1 time of LiTFSI was fitted to be 118.90 s (Figure S6b).

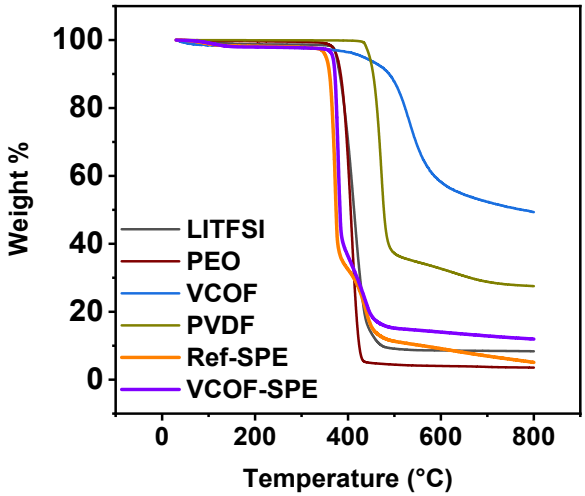

Figure S7. TGA curves of LiTFSI, PEO, VCOF, PVDF, Ref-SPE, and VCOF-SPE.

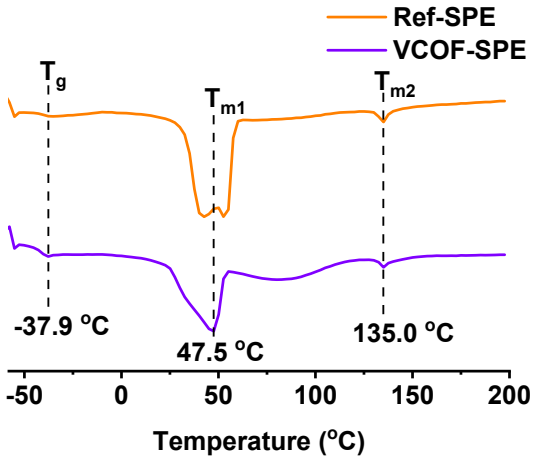

Figure S8. DSC curves of VCOF-SPE and Ref-SPE.

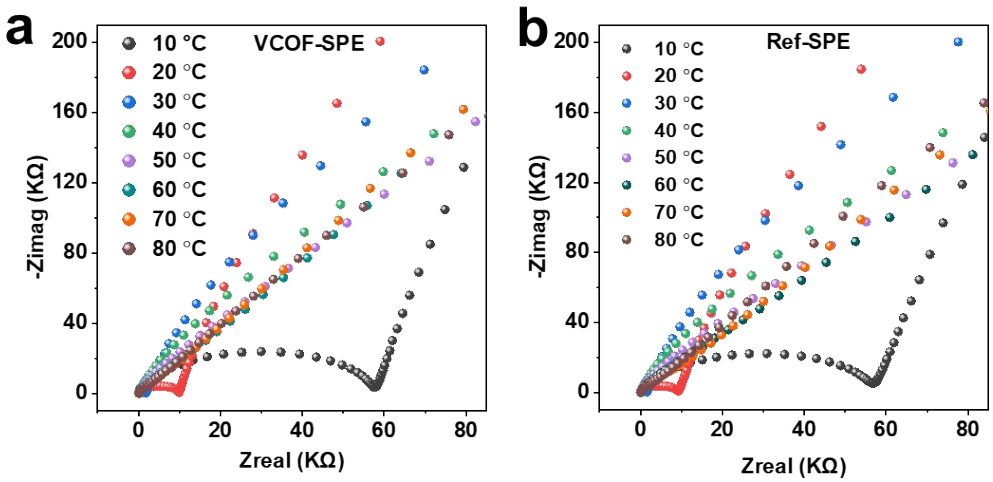

Figure S9. Electrochemical impedance spectra of VCOF-SPE (a) and Ref-SPE (b) in a temperature range of 10 – 80 °C.

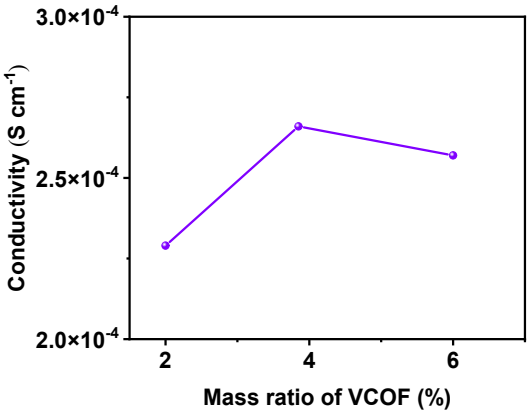

Figure. S10. The conductivity of VCOF-SPE as a function of content of VCOF-1.

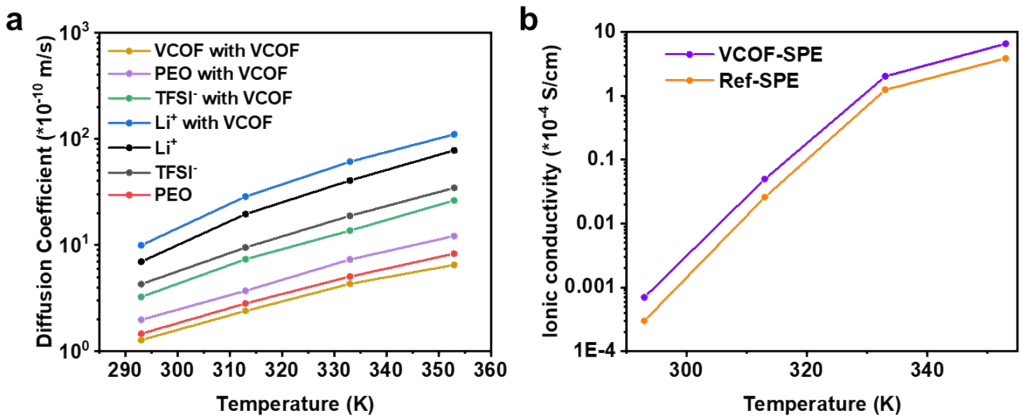

Figure. S11. (a) The diffusion coefficients of Li cations, TFSI anions, and PEO oligomers, and (b) the ion conductivities of the two modeling systems with and without VCOF-1 fragments determined from extensive atomistic simulations (Supporting Information Section 5).

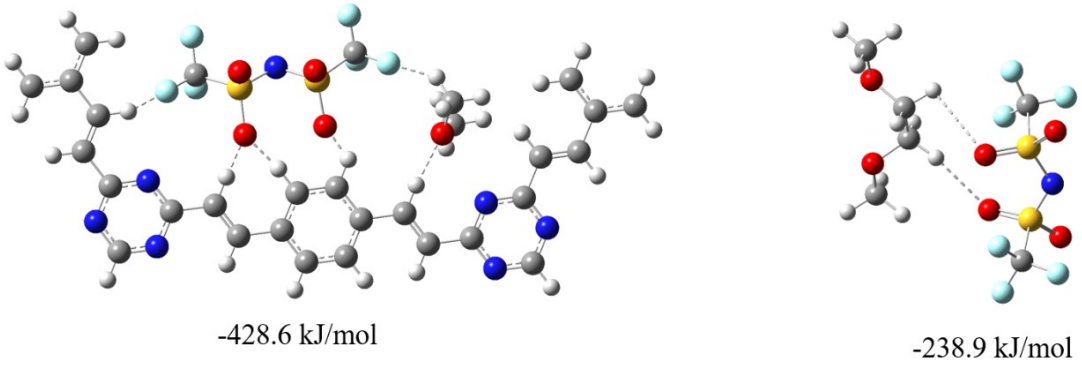

Figure. S12 Specific binding structures and the correspondent binding energies of TFSI-VCOF and TFSI-$(EO)_2$ complexes obtained from DFT calculations. (C: gray; N: blue; H: white; O: red; S: yellow; F: cyan).

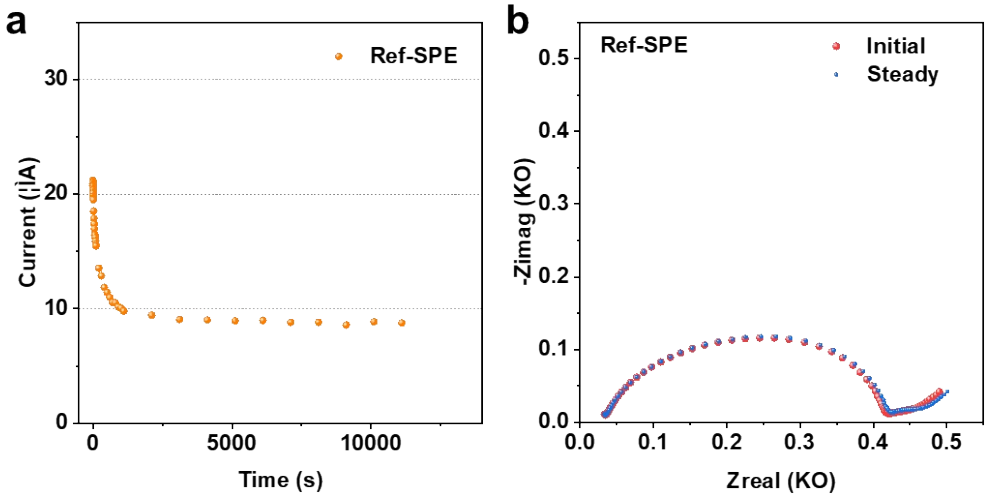

Figure S13. (a) Chronoamperometry of the Li|Ref-SPE|Li cells at the potential of 10 mV. (b) Comparison of the AC impedance of the cells before and after DC polarization at 60 °C.

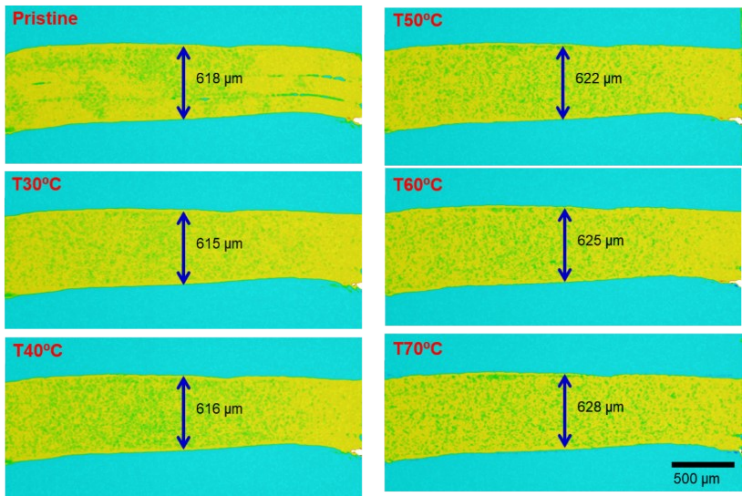

Figure S14. Cross-section views of tomography cell and corresponding average thickness at different temperatures.

The thickness of the VCOF-SPE was obtained and averaged by the ImageJ software.

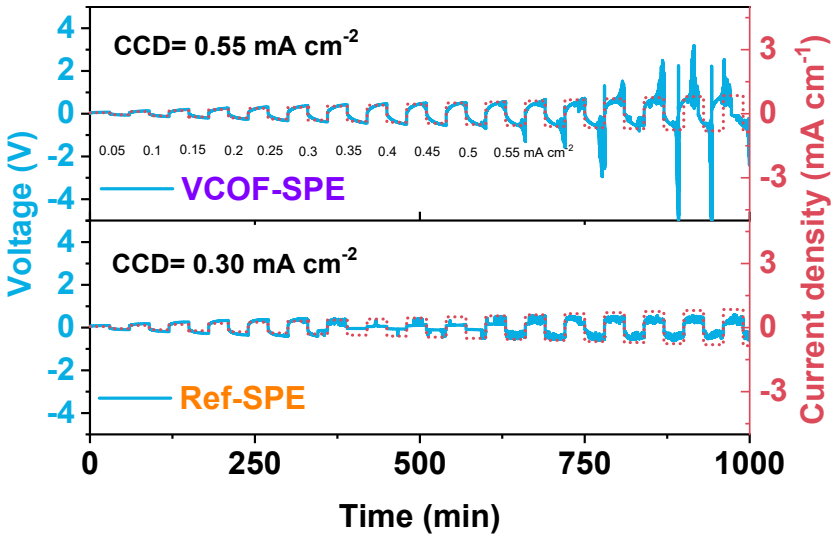

Figure S15. Galvanostatic cycling at various current densities to determine the critical current density for the VCOF-SPE membranes. The symmetric Li|VCOF-SPE|Li and Li|Ref-SPE|Li cells were charged and discharged for 30 mins at each current density (from 0.05 to 0.85 mA cm^{-2} with an interval of 0.05 mA cm^{-2}) at 60 °C.

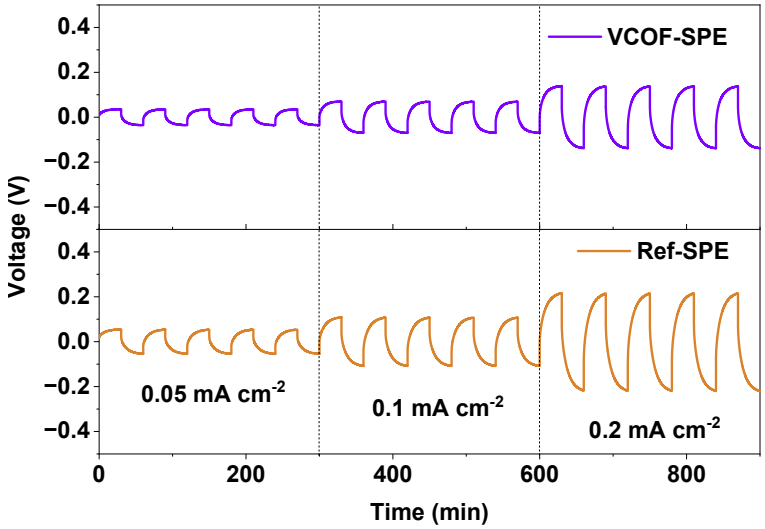

Figure S16. Rate performance of Li|VCOF-SPE|Li and Li|Ref-SPE|Li cells at different current densities at 60 °C. The cells were charged and discharged at 0.05, 0.1, and 0.2 mA cm^{-2} for 30 mins in each half-cycle, with five cycles in each current density.

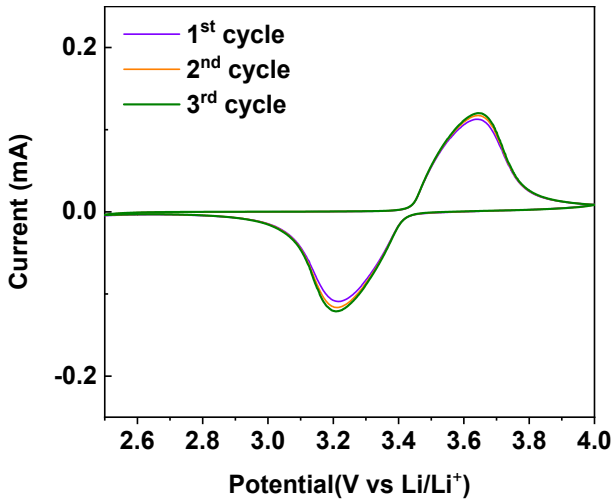

Figure S17. CV curves of LFP|VCOF-SPE|Li battery.

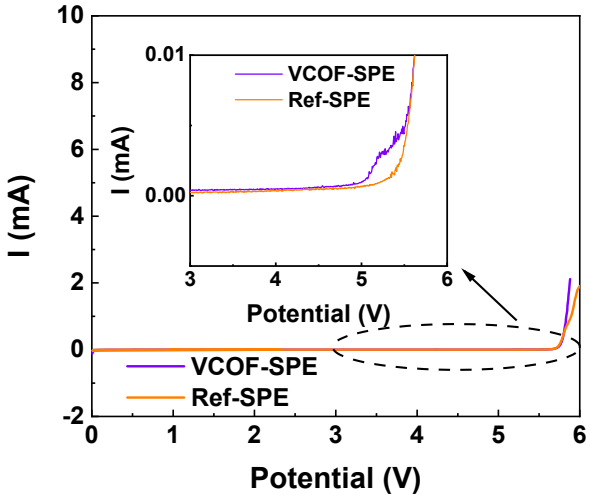

Figure S18. Electrochemical stability windows of SPEs at a scanning rate of 0.1 mV s^{-1}. Cell: Stainless steel| SPE|Li

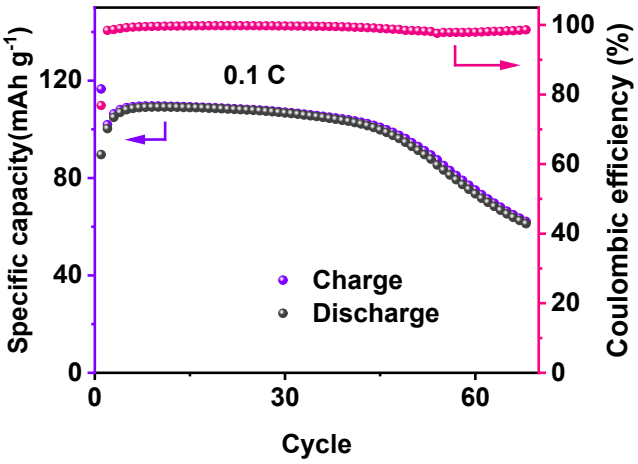

Figure S19. Cycling ability of Ref-SPE in a Li|Ref-SPE|LFP coin cell at 0.1 C current density.

References

1 A. Acharjya, P. Pachfule, J. Roeser, F. Schmitt and A. Thomas, *Angew. Chemie Int. Ed.*, 2019, **58**, 14865–14870.

2 V. St-Onge, M. Cui, S. Rochon, J.-C. Daigle and J. P. Claverie, *Commun. Mater.*, 2021, **2**, 83.

3 K. Dong, M. Osenberg, F. Sun, H. Markötter, C. J. Jafta, A. Hilger, T. Arlt, J. Banhart and I. Manke, *Nano Energy*, 2019, **62**, 11–19.

4 C. T. Rueden, J. Schindelin, M. C. Hiner, B. E. DeZonia, A. E. Walter, E. T. Arena and K. W. Eliceiri, *BMC Bioinformatics*, 2017, **18**, 529.

5 O. Sheng, J. Zheng, Z. Ju, C. Jin, Y. Wang, M. Chen, J. Nai, T. Liu, W. Zhang, Y. Liu and X. Tao, *Adv. Mater.*, 2020, **32**, 2000223.

6 P. G. Bruce and C. A. Vincent, *J. Electroanal. Chem. Interfacial Electrochem.*, 1987, **225**, 1–17.

7 H. Chen, D. Adekoya, L. Hencz, J. Ma, S. Chen, C. Yan, H. Zhao, G. Cui and S. Zhang, *Adv. Energy Mater.*, 2020, **10**, 2000049.